Brain Structure and Function (2021) 226:1727–1741
https://doi.org/10.1007/s00429-021-02282-z

ORIGINAL ARTICLE

A fully segmented 3D anatomical atlas of a lizard brain

Daniel Hoops[1,2] · Hanyi Weng[1] · Ayesha Shahid[1] · Philip Skorzewski[1] · Andrew L. Janke[3] · Jason P. Lerch[1,2,4] · John G. Sled[1,2]

Received: 17 November 2020 / Accepted: 18 April 2021 / Published online: 30 April 2021

Abstract

As the relevance of lizards in evolutionary neuroscience increases, so does the need for more accurate anatomical references. Moreover, the use of magnetic resonance imaging (MRI) in evolutionary neuroscience is becoming more widespread; this represents a fundamental methodological shift that opens new avenues of investigative possibility but also poses new challenges. Here, we aim to facilitate this shift by providing a three-dimensional segmentation atlas of the tawny dragon brain. The tawny dragon (*Ctenophorus decresii*) is an Australian lizard of increasing importance as a model system in ecology and, as a member of the agamid lizards, in evolution. Based on a consensus average 3D image generated from the MRIs of 13 male tawny dragon heads, we identify and segment 224 structures visible across the entire lizard brain. We describe the relevance of this atlas to the field of evolutionary neuroscience and propose further experiments for which this atlas can provide the foundation. This advance in defining lizard neuroanatomy will facilitate numerous studies in evolutionary neuroscience. The atlas is available for download as a supplementary material to this manuscript and through the Open Science Framework (OSF; https://doi.org/10.17605/OSF.IO/UJENQ).

Keywords Reptile · Magnetic resonance imaging · Agamid · Evolutionary neuroscience · Segmentation · Registration

Introduction

A recent surge in neuroevolutionary research using reptile species reflects the increasing realization that the variation among extant reptiles makes this a powerful group with which to tease apart the patterns and processes that have shaped the vertebrate brain (Nomura et al. 2013; Roth et al. 2019; Hoops 2018; Reiter et al. 2017; Szabo et al. 2020; Macrì et al. 2019). This understanding has been driven in part by the use of three-dimensional imaging techniques to gather neuroanatomical data in reptiles (Macrì et al. 2019; Behroozi et al. 2018; Hoops et al. 2017a, b; Luo et al. 2009; Hughes et al. 2016). High-resolution structural MRI rapidly provides detailed neuroanatomical information over the whole brain and overcomes some of the limitations of traditional histological methods such as tissue destruction, shape distortion caused by processing, and labor-intensive protocols (Nieman 2005). While work with lizard species to date has focused on analysis of fixed specimens, MRI can also be used to gather neuroanatomical data from living animals, enabling longitudinal analysis. Therefore, this technique has strong potential to link our existing understanding of reptile neuroanatomy with parallel developments in the understanding of cognitive evolution in reptiles.

Despite the strong potential, the use of MRI in reptiles to expand neuroevolutionary research poses significant challenges. Chief among these is the interpretation of the neuroanatomical structures visible in MRI images with reference to available brain atlases based on histology. Whereas traditional histology makes use of optical stains that bind with varying degrees of specificity to macromolecular components

This work is dedicated to the memory of Jeremy F. P. Ullmann, who first convinced me that this project was possible.–Daniel Hoops.

✉ Daniel Hoops
daniel.hoops@mail.mcgill.ca

1 Mouse Imaging Centre, The Hospital for Sick Children, Toronto, ON, Canada

2 Department of Medical Biophysics, University of Toronto, Toronto, ON, Canada

3 Center for Advanced Imaging, The University of Queensland, Brisbane, QLD, Australia

4 Wellcome Centre for Integrative Neuroimaging, FMRIB, Nuffield Department of Clinical Neurosciences, University of Oxford, Oxford, UK

of tissue, MRI contrast is derived from water molecules and their interactions with adjacent cellular structures. To aid in the interpretation of MR images of reptile neuroanatomy, a brain atlas that identifies neuroanatomical structures on a series of two-dimensional MR images has recently been published (Hoops et al. 2018). Such 2D atlases, while useful as an aid to visual assessment of MR images, are limiting for quantitative analysis of brain morphology. In other species, most notably humans (Dickie et al. 2017) and in a range of other model organisms (Dorr et al. 2008; Frey et al. 2011), 3D atlases, where the whole brain has been segmented into individual neuroanatomical structures, have been used to identify relationships between neuroanatomic, genetic, and environmental factors.

A structural segmentation atlas can enhance the analysis of neuroanatomical MRI data by (1) supporting the automated analysis of new MRI datasets by algorithmically assigning each voxel in the three-dimensional image to a brain structure; (2) enabling the automated calculation of various morphological metrics of brain structures, for example volume and surface area; and (3) aiding in the identification of statistical variations in brain anatomy between groups of interest. Creating a 3D segmentation atlas comes with its own challenges, however, and requires a detailed understanding of reptile neuroanatomy, access to high-resolution MRIs for a species of interest, and access to specialized software algorithms that can generate a consensus model brain image from numerous MRIs.

Here, we provide, following meticulous and thorough study, a structural segmentation atlas for the tawny dragon (*Ctenophorus decresii*), an agamid lizard (Hamilton et al. 2015). This work is designed to complement and advance upon previous reptile brain atlases, including the recently published atlas of tawny dragon (Hoops et al. 2018) that was based on MRI but not on a three-dimensional segmentation of the entire brain. The present atlas is based on the same consensus average MR model as in Hoops et al. (2018), which was generated from MRIs of 13 adult male tawny dragon brains and has a voxel size of $(20\ \mu m)^3$. In our atlas, we identified and traced 224 structures in three dimensions using a combination of image contrast and anatomical markers to bind each anatomical region. We show that the three-dimensional structure of complex brain regions and structural groups can be easily visualized using this approach. This atlas can be used for the automated measurement of lizard brain MRIs and is freely available for download, as is the model on which it is based.

Methods

Detailed methods regarding specimen acquisition and processing, MRI acquisition, and consensus model generation can be found in Hoops et al. (2018).

Specimens

Thirteen adult male tawny dragons (*Ctenophorus decresii*) were collected in the southern Flinders Ranges, Australia. All individuals were collected from within one of the distinct genetic lineages known for this species (McLean and Stuart-Fox 2014; Stuart-Fox et al. 2021). As they were collected from the wild, they were not further matched beyond being adult and male. The dragons were brought to the Australian National University in Canberra, Australia where they were housed in outdoor enclosures with ad libitum access to food (wild insects and domestic crickets) and water.

Each lizard was euthanized using an intraperitoneal injection of 100 mg/kg sodium pentobarbital and an equal volume of 2 mg/mL lignocaine to relieve any discomfort from the injection. The lizards were then intracardially perfused according to the protocol in Hoops (2015), using paraformaldehyde as the fixative agent. Magnevist was added as a paramagnetic contrast agent at a concentration of 1% to improve contrast in MRI. Brains were removed from the skulls and stored in phosphate-buffered saline with 0.1% Magnevist and 0.05% sodium azide at 4 °C until imaging.

For imaging, brains were stabilized in a custom-made brain holder and immersed in Fomblin. Images were acquired using a Bruker Avance 11.74 T wide-bore spectrometer using the following parameters: a 3D fast gradient-echo sequence having T1 and T2* weighting with a repetition time of 40 ms, a flip angle of 58.4°, an echo time of 8 ms, a field-of-view of $11 \times 11 \times 16$ mm, and a matrix size of $110 \times 110 \times 160$. Each resulting image had an isotropic resolution of $(50\ \mu m)^3$.

Each brain image was manually masked to achieve consistent coverage of all brain regions and nerve endings. Olfactory bulbs could not be stabilized in the scanner with respect to the rest of the brain, and so were excluded from analysis by masking. A consensus model of the 13 brains was then generated as described in Janke and Ullmann (2015). The final consensus model was constructed with a voxel size of $(20\ \mu m)^3$ and includes the entire brain except for the olfactory bulbs.

Segmentation of brain structures

224 structures were manually segmented on the consensus model of the tawny dragon brain. The segmentation was performed by three individuals (HW, AS, and PS), each of whom was responsible for a different suite of structures. The three segmentations were then merged using the MINC computing environment (Vincent et al. 2016) and

the fully segmented brain was then thoroughly checked for overall consistency and accuracy in all three planes by two individuals: first by HW and then by DH. Any points of ambiguity were identified and discussed by HW and DH and the literature was consulted as required (Hoops et al. 2018; Corral et al. 1990; Donkelaar 1998; Greenberg 1982; Butler and Northcutt 1973; Northcutt 1967; Smeets et al. 1986; Cruce 1974; Cruce and Newman 1981; Donkelaar et al. 2012; Schwab 1979; Díaz and Glover 2002; Medina et al. 1992; Powers and Reiner 1980; Billings et al. 2020). The operational criteria for identifying the boundaries of brain regions were defined in terms of differences in signal intensity and/or their location with reference to anatomical landmarks.

Segmentation was performed using the software package Display (http://www.bic.mni.mcgill.ca/software/Display/Display.html, Montreal Neurological Institute, Montreal, Canada). Regions were segmented using a three-panel view, such that progress could be viewed in coronal, sagittal, and transverse orientations simultaneously. Therefore, brain regions were segmented in all three planes concurrently, and no one plane took priority. The nomenclature and abbreviations we use here follow Hoops et al. (2018).

Statistical analysis

We used our segmentation atlas to measure each brain region in each of the 13 MRIs that were used to generate the tawny dragon brain model (Chakravarty et al. 2013). To do this, we used the multiple automatically generated templates of different brains (MAGeT Brain) automated procedure to map the segmentation atlas to each individual brain. The procedure relies on the spatial transforms relating the individual images to the consensus average. First, the atlas is transformed to match each brain. These 13 labelled images are then combined using a multi-atlas labelling procedure with voxel voting to refine these labels for each brain (Collins and Pruessner 2010). For an in-depth account of the MAGeT procedure, see Chakravarty et al. (2013).

We then used the R (2014) package metaphor (Viechtbauer 2010) to calculate the log-transformed coefficient of variation for each brain region across the 13 samples as a measure of between-individual variation. Brain regions for whom the coefficient of variation falls above the 95% prediction interval of all brain regions are considered to be more variable than expected, while those that fall below the 95% prediction interval are less variable than expected. This serves as a demonstration of the power of a segmentation atlas for rapidly generating neuroanatomical data for analysis.

Our segmentation atlas of the lizard brain is freely available as a supplementary material to this manuscript, as is the lizard brain MRI model on which it is based. All these materials are also available, in addition to the code and data used in this manuscript, through the Open Science Framework (OSF; https://doi.org/10.17605/OSF.IO/UJENQ).

Results

The process described above resulted in a detailed neuroanatomical segmentation atlas of the male tawny dragon (*Ctenophorus decresii*) brain. The atlas consists of 224 structures and is freely available to researchers and the public via download in the supplementary materials of from the Open Science Framework (OSF; https://doi.org/10.17605/OSF.IO/UJENQ). Figure 1 shows serial sections through our atlas in the coronal plane, Fig. 2 in the transverse plane, and Fig. 3 in the sagittal plane. Figure 4 shows the atlas projected onto a 3D surface view of the tawny dragon brain. We have also included a basic hierarchy of the anatomical groups of these 224 structures according to the neuromeric model of brain development (Supplementary Table 1).

We present a table of the volumes of each region for each of the 13 tawny dragon brain images that make up the model, demonstrating the power of our atlas for efficient measurement of brain regions (Table 1). As these brains are from wild-collected dragons, we expect more inter-individual variation than in inbred strains of model organisms. However, as the image registration algorithm removes these inter-individual differences when constructing a consensus average image, this added population variability does not degrade quality of the final atlas. Each 3D image was reviewed following alignment to verify that the anatomical boundaries aligned with the structures seen on the consensus average image. To look specifically at variation between individuals, we calculated the log-transformed coefficient of variation for each brain region as a measure of variation between individuals, and Fig. 5 illustrates which brains regions are more or less variable than expected.

As the model on which the atlas is based is bilaterally symmetric, the atlas in its native form covers only the left hemisphere and is defined on a voxel grid that brackets the mid-plane. Figure 6a shows the optic system of the lizard brain in the left hemisphere. The atlas can easily be reflected to the right hemisphere to identify and measure structures in that hemisphere or bilaterally. Figure 6b shows several of the brain's commissures. They have been reflected into the right hemisphere to demonstrate how they appear bilaterally.

The primary determinant of structural boundaries between adjacent brain regions is change in voxel intensity (i.e., image contrast); however, at some boundaries, such changes are not detected. These boundaries were delineated using anatomical landmarks identified by careful examination of the published literature. Furthermore, while a particular region may be clearly delineated by voxel intensity

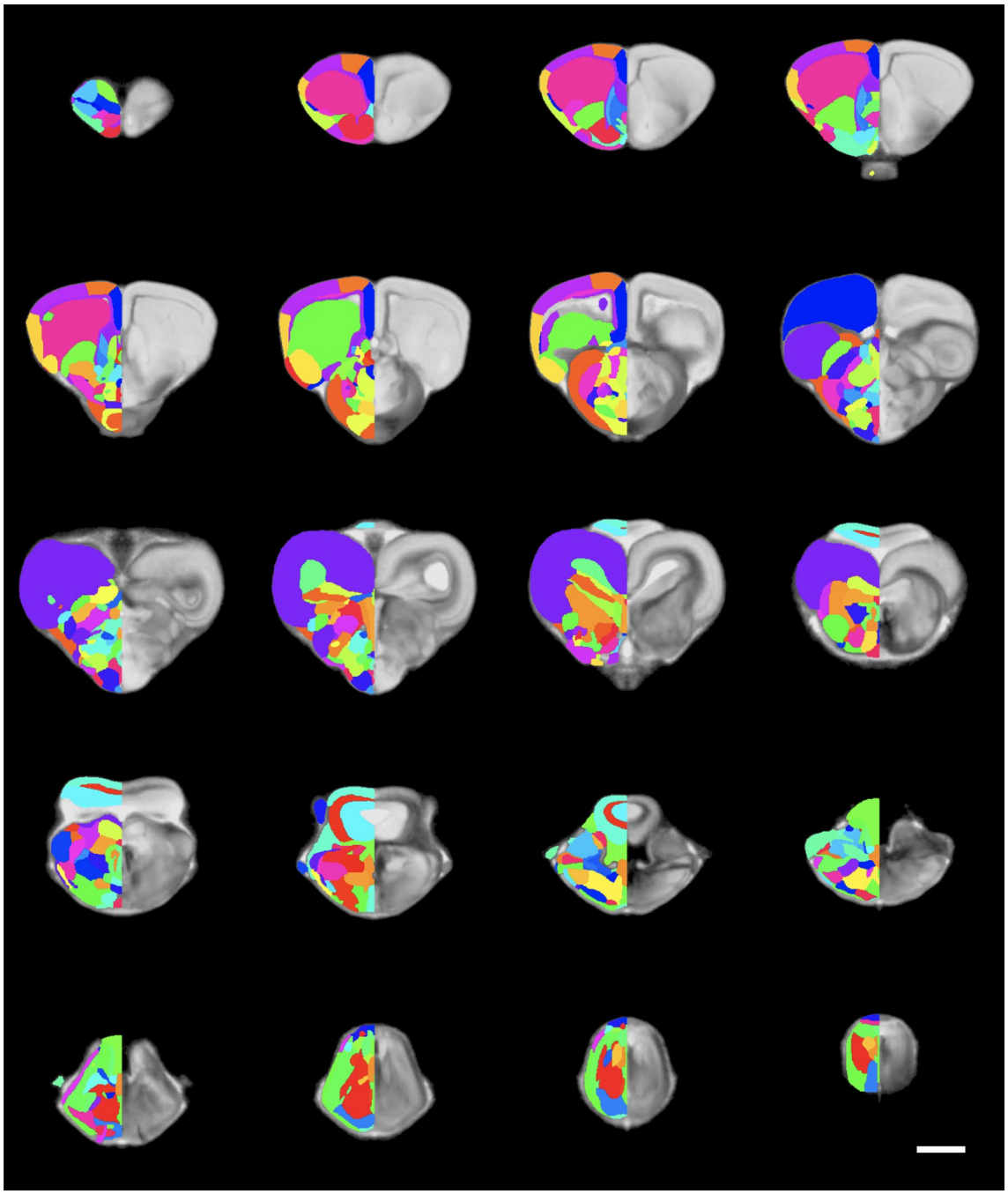

Fig. 1 Sequential coronal sections through the MRI model of the tawny dragon (*Ctenophorus decresii*) brain reveal the labelling of our lizard brain atlas. Each segment (brain region or structure) has been randomly assigned a colour. Colours will not be consistent across devices or applications, though segment identification numbers will remain constant. Coronal sections show the segmentation (hemisphere on the left) and the brain model (hemisphere on the right). The most anterior (top left) section shows the plane $y = -3.25$ mm and each section is 333 µm or 17 voxels posterior to the previous section. Scale bar at bottom right = 1 mm

in one of the three two-dimensional visualization planes (coronal, sagittal, and horizontal), it does not necessarily follow that the region is clearly identifiable by intensity across all three planes. As segmentation in all three planes is required to achieve accurate and precise boundaries between structures, we provide in Table 1 a summary of where contrast-based segmentation was the primary determinant of boundary location, and where literature-based segmentation (i.e., anatomical landmarks) was primarily used.

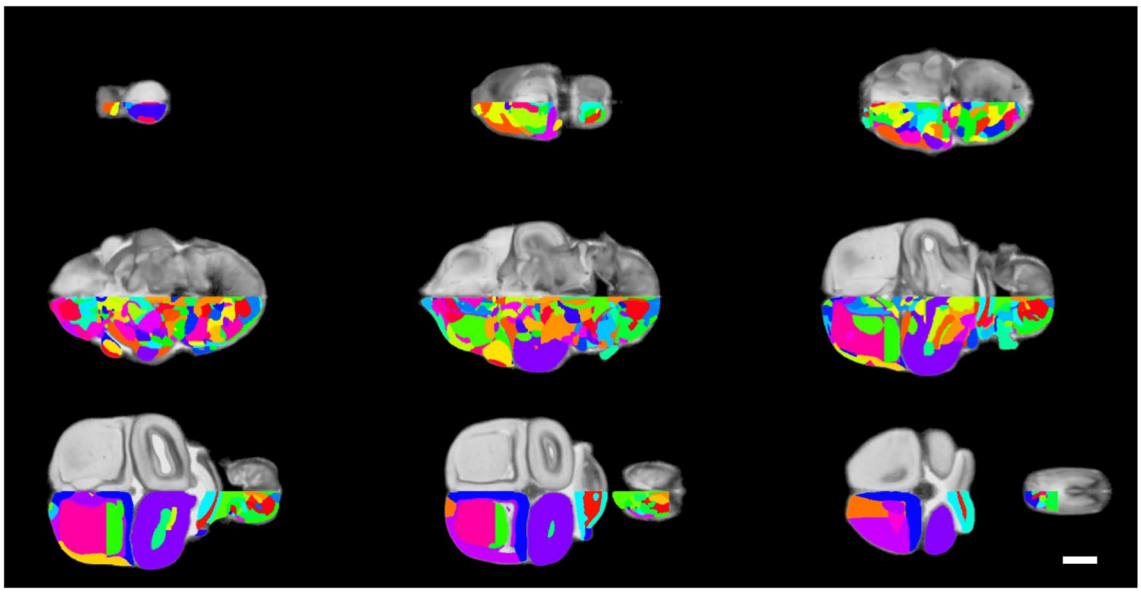

Fig. 2 Sequential transverse sections through the MRI model of the tawny dragon (*Ctenophorus decresii*) brain reveal the labelling of our lizard brain atlas. Each segment (brain region or structure) has been randomly assigned a colour. Colours will not be consistent across devices or applications, though segment identification numbers will remain constant. Transverse sections show the brain model (top hemisphere) and the segmentation (bottom hemisphere). The most ventral section (top left) shows the plane $z = -1.88$ mm and each section is 444 µm or 22 voxels dorsal to the previous one. Scale bar at bottom right = 1 mm

Although the primary reference upon which this atlas is based is Hoops et al. (2018), several additional atlases were consulted. These include references for the entire lizard brain (Corral et al. 1990; Donkelaar 1998; Medina et al. 1992), for the telencephalon (Greenberg 1982; Northcutt 1967; Smeets et al. 1986), for the diencephalon (Butler and Northcutt 1973; Cruce 1974), and for the hindbrain (Cruce and Newman 1981; Donkelaar et al. 2012; Schwab 1979; Díaz and Glover 2002). We also examined atlases available for other reptile groups: turtles (Powers and Reiner 1980) and crocodilians (Billings et al. 2020).

Discussion

Here, we present a three-dimensional atlas of a lizard brain consisting of 224 identified and delineated structures. The model on which we base our atlas is a non-linear average of the brains of 13 male tawny dragons (*Ctenophorus decresii*). Using a non-linear average instead of basing our atlas on the image of a single brain, we were able to greatly increase the contrast and resolution [to $(20\ \mu m)^3$]. This allowed us to identify a greater number of structures compared to other MRI-based atlases based on individual images. Table 1 lists the structures included in our atlas, as well as their acronyms and labels. The names and acronyms are consistent with Hoops et al. (2018), and most are also consistent with ten Donkelaar (1998). As ten Donkelaar (1998) is a review which summarizes all reptile neuroanatomical literature up to 1995, this consistency allows users to easily refer to our atlas when delving into the lizard neuroanatomical literature.

Progress in reptile neuroanatomy

In the past 20 years there has been a great expansion in squamate brain research. This literature can be broadly grouped into two distinct areas. First, many neuroscience researchers continue fundamental research on the structure, connectivity, and neurochemistry of the squamate brain from a predominantly anatomical perspective. These studies use methods such as tract-tracers and immunohistochemistry to examine anatomy. This work is of immense value as it provides the foundation from which we can examine possible homologies between the nervous system of squamates and other better-known vertebrate groups, and ultimately understand the origins of the vertebrate brain. Second, a newer stream has emerged that focuses on linking brain structure and chemistry with behaviour, sociality, cognition, and learning. By identifying particular aspects of behaviour, ecology, or evolution in squamates, we can "work backwards" to try to link these to underlying brain function. Unique aspects of ecology, for example the link between throat colour and mating strategy in the tawny dragon (Yewers et al. 2016), create ideal systems for examining the neural basis of behaviour and its evolution. As our appreciation for the behavioural

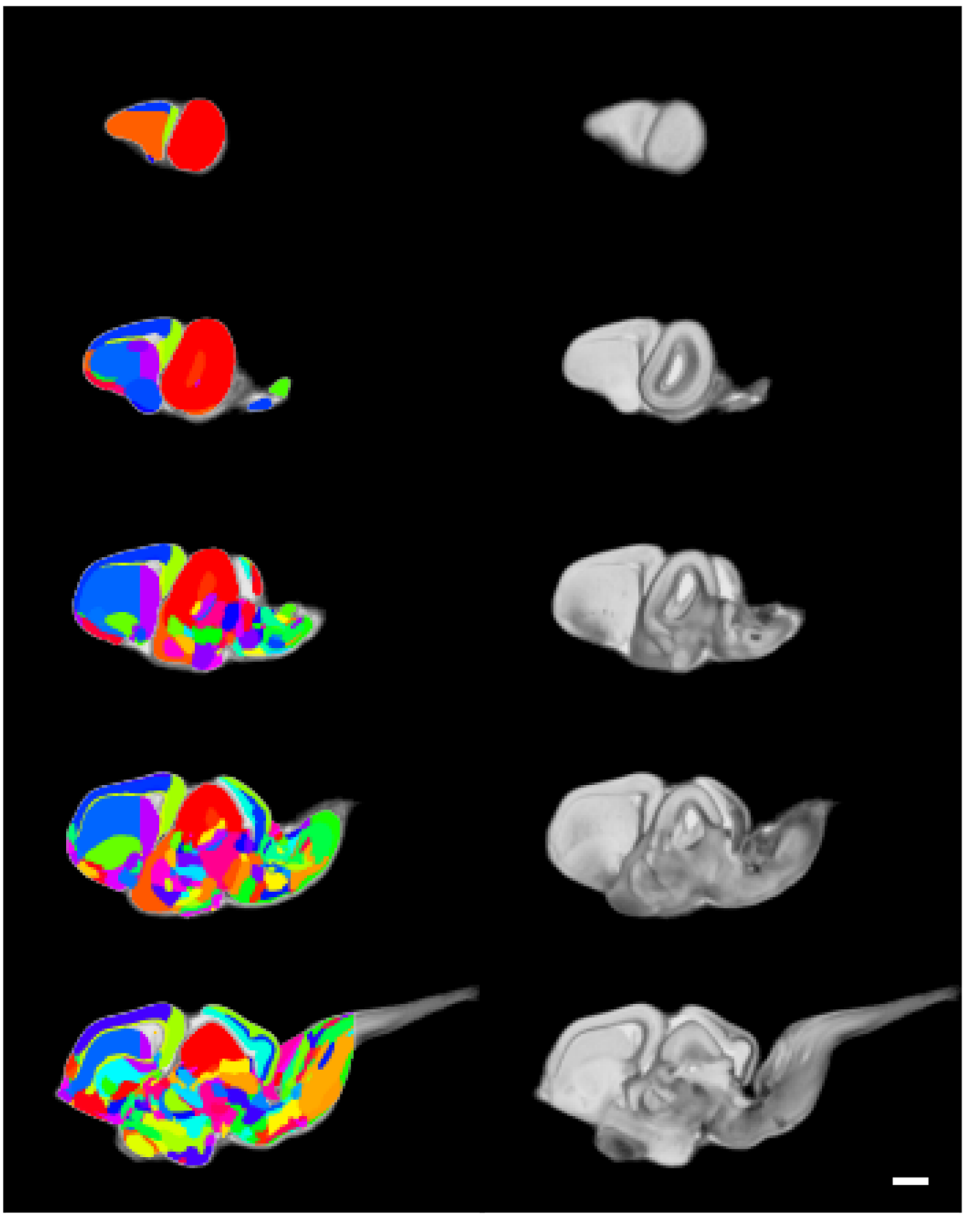

Fig. 3 Sequential sagittal sections through the MRI model of the tawny dragon (*Ctenophorus decresii*) brain reveal the labelling of our lizard brain atlas. Each segment (brain region or structure) has been randomly assigned a colour. Colours will not be consistent across devices or applications, though segment identification numbers will remain constant. Sagittal sections showing the segmentation (left-hand column) and the brain model (right-hand column). The most lateral section (top section of both rows) shows the plane $x = 2.50$ mm and each section is 500 µm or 25 voxels medial to the previous one. Scale bar at bottom right = 1 mm

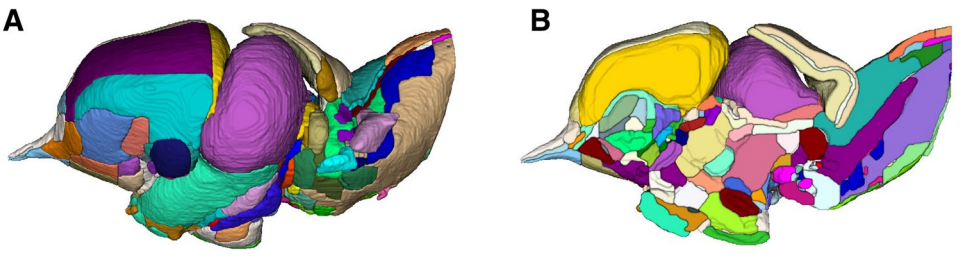

Fig. 4. 3D projection of our segmentation atlas of the tawny dragon (*Ctenophorus decresii*) brain showing the lateral surface (**a**) and the medial surface (**b**) of the left hemisphere. Scale bar at bottom right = 1 mm

and cognitive complexity of reptiles increases, new opportunities to study the neural underpinnings of behaviour and cognition are constantly emerging.

A fundamental tool necessary to link cognition and behaviour with neuroscience, the brain atlas, has not progressed in this time. In fact, the most widely used lizard brain atlas dates from 1982 (Greenberg 1982). In terms of resolution, the atlases that have been available for lizards are inferior to the available atlases for other vertebrate groups. It is significant, therefore, that the two reptile brain atlases

Table 1 Neuroanamotical structures identified in our segmentation atlas

Abbrev.	Structure	Label	Coronal	Sagittal	Horizontal	Volume^{+}
4v	Fourth ventricle	175	CB	CB	CB	0.702 ± 0.11
a	Alveus	326	CB	CB	CB	0.950 ± 0.12
A8	Catecholaminergic cell group A8	106	CB	CB	CB	0.127 ± 0.01
ac	Anterior commissure	252	CB	CB	CB	0.040 ± 0.00
Acc	Accumbens nucleus	318	CB	CB	CB	0.402 ± 0.04
Aco	Angular cochlear nucleus	20	CB	CB	CB	0.025 ± 0.00
ADVR	Anterior dorsal ventricular ridge	323	CB	CB	CB	3.856 ± 0.46
AH	Anterior or alar hypothalamic area	180	CB	CB	CB	0.112 ± 0.01
AON	Anterior olfactory nucleus	327	CB	CB	CB	0.083 ± 0.02
apc	Anterior pallial commissure	319	CB	CB	CB	0.021 ± 0.00
Arc	Arcuate nucleus	189	CB	CB	CB	0.023 ± 0.00
Asp	Anterior septal nucleus	328	CB	CB	CB	0.205 ± 0.03
Au	Auricle	304	CB	CB	CB	0.062 ± 0.01
B	Bischoff's nucleus	86	CB	CB	CB	0.009 ± 0.00
BAC	Bed nucleus of the anterior commissure	220	CB	CB	CB	0.041 ± 0.00
bc	Brachium conjunctivum	152	CB	CB	CB	0.004 ± 0.00
BOT	Nucleus of the basal optic tract	139	CB	CB	CB	0.143 ± 0.01
bot	Basal optic tract	140	CB	CB	CB	0.079 ± 0.01
BSTl	Bed nucleus of the stria terminalis, lateral part	312	CB	CB	CB	0.169 ± 0.02
BSTm	Bed nucleus of the stria terminalis, medial part	310	CB	CB	CB	0.051 ± 0.01
CAq	Cerebral aqueduct	172	CB	CB	CB	0.024 ± 0.00
Cerl	Cerebellar nucleus, lateral part	145	CB	CB	CB	0.063 ± 0.01
Cerm	Cerebellar nucleus, medial	136	CB	CB	CB	0.081 ± 0.01
CG	Central gray	107	CB	CB	CB	0.439 ± 0.03
CP	Choroid plexus	316	CB	CB	CB	0.008 ± 0.00
CPDmC	Cell plate of the dorsomedial cortex	337	CB	CB	CB	0.055 ± 0.01
ct	Connective tissue surrounding the alveus	97	CB	CB	CB	0.040 ± 0.01
DB	Nucleus of the diagonal band	348	CB	CB	CB	0.020 ± 0.01
DC	Dorsal cortex	334	CB	CB	CB	1.216 ± 0.09
dc	Dorsal column tract	60	CB	CB	CB	0.080 ± 0.01
dco	Dorsal cochlear tract	58	CB	CB	CB	0.028 ± 0.00
DCol	Nucleus of the dorsal column, lateral part	61	CB	CB	CB	0.098 ± 0.01
DCom	Nucleus of the dorsal column, medial part	62	CB	CB	CB	0.078 ± 0.01
DcSp	Dorsal septal nucleus, central part	353	CB	CB	CB	0.010 ± 0.00
DdSp	Dorsal septal nucleus, dorsal part	322	CB	CB	CB	0.046 ± 0.00
DH	Dorsal horn of the spinal cord	6	CB	CB	CB	0.024 ± 0.00
Dl	Dorsolateral thalamic nucleus	75	CB	CB	CB	0.950 ± 0.08
Dl	Dorsolateral thalamic nucleus	215	CB	CB	CB	0.087 ± 0.01
DLA	Dorsolateral amygdala	309	CB	CB	CB	0.047 ± 0.01
DlH	Dorsolateral hypothalamic nucleus	181	CB	CB	CB	0.193 ± 0.02
Dm	Dorsomedial thalamic nucleus	212	CB	CB	CB	0.199 ± 0.02
DmC	Dorsomedial cortex	335	CB	CB	CB	0.790 ± 0.07
DmH	Dorsomedial hypothalamic nucleus	182	CB	CB	CB	0.099 ± 0.01
DPt	Dorsal pretectal nucleus	149	CB	CB	CB	0.147 ± 0.02
DSp	Dorsal septal nucleus	324	CB	CB	CB	0.073 ± 0.01
DSt	Dorsal striatum	308	CB	CB	CB	0.889 ± 0.11
DTN	Dorsal tegmental nucleus	137	CB	CB	CB	0.086 ± 0.01
Epa	Entopeduncular nucleus, anterior part	197	CB	CB	CB	0.023 ± 0.00
Epp	Entopeduncular nucleus, posterior part	161	CB	CB	CB	0.091 ± 0.01
Ept	External pretectal nucleus	164	CB	CB	CB	0.032 ± 0.00

Table 1 (continued)

Abbrev.	Structure	Label	Coronal	Sagittal	Horizontal	Volume^{+}
EW	Nucleus of Edinger-Westphal	108	CB	CB	CB	0.006 ± 0.00
f	Fornix	225	CB	CB	CB	0.036 ± 0.00
Fim	Fimbria	317	CB	CB	LB	0.037 ± 0.00
fr	Fasciculus retroflexus	198	CB	CB	CB	0.029 ± 0.00
gl	Glomerular layer of the cerebellum	303	CB	CB	CB	0.658 ± 0.05
GP	Globus pallidus	350	CB	CB	CB	0.057 ± 0.01
Hb	Habenula	207	CB	CB	CB	0.019 ± 0.00
HbL	Lateral habenula	210	CB	CB	CB	0.029 ± 0.00
HbM	Medial habenula	208	CB	CB	CB	0.019 ± 0.00
hc	Habenula commissure	209	CB	CB	CB	0.004 ± 0.00
iaf	Internal arcuate fibres	74	CB	CB	CB	0.017 ± 0.00
Ic	Intercollicular nucleus	127	CB	CB	CB	0.206 ± 0.02
IF	Nucleus of the infima commissure	80	CB	CB	CB	0.008 ± 0.00
if	Infima commissure	79	CB	CB	CB	0.015 ± 0.01
III	Nucleus of the oculomotor nerve	101	CB	CB	CB	0.067 ± 0.01
IIId	Nucleus of the oculomotor nerve, dorsal part	102	CB	CB	CB	0.040 ± 0.01
IIIv	Nucleus of the oculomotor nerve, ventral part	103	CB	CB	CB	0.012 ± 0.00
IMLF	Interstitial nucleus of the medial longitudinal fasciculus	159	CB	CB	CB	0.038 ± 0.01
iot	Intermediate olfactory tract	237	CB	CB	CB	0.016 ± 0.00
Ipd	Interpeduncular nucleus, dorsal part	109	CB	CB	CB	0.039 ± 0.00
Ipd	Interpeduncular nucleus, ventral part	110	CB	CB	CB	0.074 ± 0.01
Ira	Inferior raphe nucleus	21	CB	CB	CB	0.222 ± 0.03
IRFv	Ventral nucleus of the inferior reticular formation	53	CB	CB	CB	0.454 ± 0.08
IsD	Isthmic nucleus, diffuse part	111	CB	CB	CB	0.063 ± 0.01
IsM	Isthmic nucleus, magnocellular part (pre-isthmic or mesencephalic)	112	CB	CB	CB	0.160 ± 0.01
IsP	Isthmic nucleus, parvocellular part	113	CB	CB	CB	0.072 ± 0.01
ISp	Inferior septal nucleus	325	CB	CB	CB	0.059 ± 0.01
IV	Nucleus of the trochlear nerve	105	CB	CB	CB	0.088 ± 0.01
LA	Lateral amygdala	307	CB	CB	CB	0.063 ± 0.01
LC	Lateral cortex	332	CB	CB	CB	0.553 ± 0.05
lfb	Lateral forebrain bundle	201	CB	CB	CB	0.438 ± 0.05
lfbd	Lateral forebrain bundle, dorsal part	142	CB	CB	CB	0.125 ± 0.01
lfbv	Lateral forebrain bundle, ventral part	153	CB	CB	CB	0.092 ± 0.01
LGd	Lateral geniculate nucleus, dorsal part	216	CB	CB	CB	0.070 ± 0.01
LGv	Lateral geniculate nucleus, ventral part	203	CB	CB	CB	0.298 ± 0.03
LHA	Lateral hypothalamic area	183	CB	CB	CB	0.291 ± 0.02
LJc	Lateral juxtacommissural nucleus	165	CB	CB	CB	0.119 ± 0.01
ll	Lateral lemniscus	144	CB	CB	CB	0.070 ± 0.01
LL	Nucleus of the lateral lemniscus	14	CB	CB	CB	0.063 ± 0.01
LLd	Nucleus of the lateral lemniscus, dorsal part	115	CB	CB	CB	0.044 ± 0.01
LLv	Nucleus of the lateral lemniscus, ventral part	116	CB	CB	CB	0.067 ± 0.01
LoC	Locus coeruleus	117	CB	CB	CB	0.181 ± 0.02
lot	Lateral olfactory tract	349	CB	CB	CB	0.026 ± 0.01
LPo	Lateral preoptic area	205	CB	CB	LB	0.005 ± 0.00
LSp	Lateral septal nucleus	240	CB	CB	CB	0.169 ± 0.02
LTN	Lateral tuberal nucleus	190	CB	CB	CB	0.034 ± 0.00
lv	Lateral vestibulospinal tract	25	CB	CB	CB	0.082 ± 0.01
MA	Medial amygdala	248	CB	CB	CB	0.051 ± 0.01
Mam	Mammillary nuclei	192	CB	CB	CB	0.043 ± 0.00
MC	Medial cortex	234	CB	CB	CB	2.063 ± 0.21

Table 1 (continued)

Abbrev.	Structure	Label	Coronal	Sagittal	Horizontal	Volume^{+}
MCo	Magnocellular cochlear nucleus	44	CB	CB	CB	0.077 ± 0.01
Me	Medial thalamic nucleus	196	CB	CB	CB	0.117 ± 0.01
mfb	Medial forebrain bundle	167	CB*	CB	CB	0.286 ± 0.03
MJc	Medial juxtacommissural nucleus	171	CB	CB	CB	0.016 ± 0.00
ML	Molecular layer of the cerebellum	301	CB	CB	CB	0.812 ± 0.07
ml	Medial lemniscus	166	CB	CB	CB	0.058 ± 0.01
mlf	Medial longitudinal fasciculus	88	CB	CB	CB	0.561 ± 0.08
MPC	Medial parvocellular nucleus	45	CB	CB	CB	0.105 ± 0.02
MPo	Medial preoptic area	218	CB	CB	CB	0.173 ± 0.02
MRF	Middle reticular formation	46	CB	CB	LB	0.495 ± 0.09
MSp	Medial septal nucleus	333	CB	CB	CB	0.055 ± 0.01
Nac	Nucleus of the anterior commissure	315	CB	CB	CB	0.027 ± 0.00
Naot	Nucleus of the accessory olfactory tract	336	CB	CB	CB	0.043 ± 0.00
Niii	Oculomotor nerve	100	CB	CB	CB	0.102 ± 0.01
Niv	Trochlear nerve	174	CB	CB	CB	0.057 ± 0.01
NLOT	Nucleus of the lateral olfactory tract	341	CB	CB	CB	0.240 ± 0.03
Npc	Nucleus of the posterior commissure	155	CB	CB	CB	0.029 ± 0.00
NSD	Nucleus of the supraoptic decussation	202	CB	CB	CB	0.020 ± 0.00
Nv	Trigeminal nerve	5	CB	CB	CB	0.046 ± 0.01
nVI	Abducens nerve	31	CB	CB	CB	0.029 ± 0.01
nVIII	Statoacoustic nerve	17	CB	CB	CB	0.243 ± 0.02
nVIIIp	Posterior root of the statoacoustic nerve	19	CB	CB	CB	0.040 ± 0.01
nVIIm	Motor root of the facial nerve	43	CB	CB	LB	0.004 ± 0.00
nVIIs	Sensory root of the facial nerve	23	CB	CB	CB	0.037 ± 0.01
nVm	Motor root of the trigeminal nerve	12	CB	CB	CB	0.033 ± 0.00
nVs	Sensory root of the trigeminal nerve	10	CB	CB	CB	0.021 ± 0.00
nVs&nVm	Sensory and motor roots of the trigeminal nerve	11	CB	CB	CB	0.088 ± 0.03
nXII	Hypoglossal nerve	35	CB	CB	CB	0.022 ± 0.00
OP	Olfactory peduncle	230	CB	CB	CB	0.000 ± 0.00
opc	Optic chiasm	221	CB	CB	CB	0.332 ± 0.03
OpT	Optic tectum	119	CB	CB	CB	6.664 ± 0.53
ot	Optic tract	173	CB	CB	CB	1.175 ± 0.12
OT	Olfactory tubercle	346	CB	CB	CB	0.020 ± 0.01
OTl	Olfactory tubercle, lateral part	339	CB	CB	CB	0.091 ± 0.01
OTm	Olfactory tubercle, medial part	242	CB	CB	CB	0.111 ± 0.02
Ov	Oval nucleus	217	CB	CB	CB	0.020 ± 0.00
p1Tg	p1 tegmental area (former pretectal reticular formation, PtR)	125	LB	LB	LB	0.170 ± 0.02
p3Tg	p3 tegmental area	224	CB	CB	CB	0.162 ± 0.01
Pb	Parabrachial nucleus	135	CB	LB	LB	0.032 ± 0.00
pc	Posterior commissure	120	CB	CB	CB	0.082 ± 0.01
PcN	Posterocentral nucleus	160	CB	CB	CB	0.048 ± 0.01
PCo	Posterior cochlear nucleus	72	CB	CB	CB	0.073 ± 0.01
PdN	Posterodorsal nucleus	150	CB	CB	CB	0.088 ± 0.01
pdt	Predorsal tract	138	CB	CB	CB	0.087 ± 0.01
PDVR	Posterior dorsal ventricular ridge	232	CB	CB	CB	1.500 ± 0.19
PH	Posterior of basal hypothalamus	185	CB	CB	CB	0.075 ± 0.01
Pl	Purkinje layer of the cerebellum	302	CB	CB	CB	0.419 ± 0.05
PmN	Posteriormedial nucleus	199	CB	CB	CB	0.048 ± 0.00
PPc	Principal precommissural nucleus	157	CB	CB	CB	0.282 ± 0.02
ppc	Postrior pallial commissure	213	CB	CB	CB	0.034 ± 0.00

Table 1 (continued)

Abbrev.	Structure	Label	Coronal	Sagittal	Horizontal	Volume^{+}
Prd	Rostrodorsal pallium	342	CB	CB	CB	0.034 ± 0.01
Prdl	Rostrodorsolateral pallium	340	CB	CB	CB	0.044 ± 0.01
Prl	Rostrolateral pallium	344	CB	CB	CB	0.040 ± 0.01
PrM	Profound mesencephalic area	121	LB	CB	LB	0.619 ± 0.07
Prm	Rostromedial pallium	343	CB	CB	CB	0.035 ± 0.01
PtE	Prethalamic eminence	195	CB	CB	CB	0.018 ± 0.00
PtG	Pretectal geniculate nucleus	151	CB	CB	CB	0.148 ± 0.01
PVN	Paraventricular nucleus	191	CB	CB	CB	0.021 ± 0.00
PvO	Paraventricular organ	188	CB	CB	CB	0.030 ± 0.00
PvON	Paraventricular organ nucleus (formerly periventricular hypothalamic nucleus	184	CB	CB	CB	0.139 ± 0.01
Pvsc	Posterior nucleus of the ventral supraoptic commissure	147	CB	CB	CB	0.234 ± 0.02
R	Red nucleus	122	CB	CB	CB	0.096 ± 0.01
r1Tg	r1 tegmental area (reticular isthmal nucleus)	134	CB	CB	CB	0.139 ± 0.02
Rmam	Retromammillary nucleus	193	CB	CB	CB	0.011 ± 0.00
rmc	Retromammillary commissure	194	CB	CB	CB	0.009 ± 0.00
Rot	Rotund nucleus	200	CB	CB	CB	0.163 ± 0.02
SAT	Striatoamygdaloid transition area	241	CB	CB	CB	0.150 ± 0.02
SC	Suprachiasmatic nucleus	219	CB	CB	CB	0.053 ± 0.01
ScO	Subcommissural organ	154	CB	CB	CB	0.012 ± 0.00
sct	Spinocerebellar tract	143	CB	CB	CB	0.137 ± 0.02
sd	Supraoptic decussation	226	CB	LB	CB	0.005 ± 0.00
sht	Septohypothalamic tract	186	CB	CB	CB	0.036 ± 0.00
sl	Spinal lemniscus	163	CB	CB	CB	0.441 ± 0.09
sm	Stria medullaris	214	CB	CB	CB	0.089 ± 0.01
SN	Substantia nigra	123	CB	CB	CB	0.135 ± 0.01
SO	Superior olivary nucleus	37	CB	CB	CB	0.100 ± 0.02
SoN	Supraoptic nucleus	222	CB	CB	CB	0.105 ± 0.01
SoT	Nucleus of the solitary tract	49	CB	CB	CB	0.215 ± 0.03
sot	Solitary tract	51	CB	CB	CB	0.026 ± 0.00
Sp	Septum	243	CB	CB	CB	0.005 ± 0.00
Sph	Spherical nucleus	305	CB	CB	CB	0.528 ± 0.05
SRa	Superior raphe nucleus	124	CB	CB	CB	0.152 ± 0.02
SRF	Superior reticular formation	141	CB	CB	LB	0.355 ± 0.04
SRl	Superior reticular area, lateral part	132	LB	LB	LB	0.182 ± 0.02
SRm	Superior reticular area, medial part	131	CB	CB	CB	0.152 ± 0.02
TA	Triangular area	223	LB	CB	CB	0.036 ± 0.00
tbtd	Tectobulbar tract, dorsal part	126	CB	CB	CB	0.121 ± 0.02
tbtv	Tectobulbar tract, ventral part	133	CB	CB	CB	0.025 ± 0.00
tc	Tectal commissure	156	CB	CB	CB	0.029 ± 0.00
tev	Tectal ventricle	169	CB	CB	CB	0.404 ± 0.06
TG	Tectal gray	146	CB	CB	CB	0.139 ± 0.01
TSc	Torus semicircularis, central nucleus	128	CB	CB	CB	0.398 ± 0.03
TSl	Torus semicircularis, laminar nucleus	129	CB	CB	CB	0.265 ± 0.03
tt	Tectothalamic tract	211	CB	CB	CB	0.019 ± 0.00
ttc	Tect, äêtegmental commissure	158	CB	CB	CB	0.012 ± 0.00
TzB	Trapezoid body	59	CB	CB	LB	0.137 ± 0.02
VA	Ventral amygdala	306	CB	CB	CB	0.025 ± 0.00
vcf	Vestibulocerebellar fibres	70	CB	CB	CB	0.021 ± 0.00
Vd	Descending nucleus of the trigeminal nerve	16	CB	CB	CB	0.797 ± 0.04
Vdl	Dorsolateral vestibular nucleus	77	CB	CB	CB	0.333 ± 0.04

Table 1 (continued)

Abbrev.	Structure	Label	Coronal	Sagittal	Horizontal	Volume+
Vdt	Descending tract of the trigeminal nerve	8	CB	CB	CB	0.089 ± 0.02
VI	Nucleus of the abducens nerve	28	CB	CB	CB	0.102 ± 0.03
VIImd	Dorsal motor nucleus of the facial nerve	50	CB	CB	CB	0.079 ± 0.02
VIImv	Ventral motor nucleus of the facial nerve	27	CB	CB	CB	0.135 ± 0.01
VL	Ventrolateral thalamic nucleus	206	CB	CB	CB	0.076 ± 0.01
VlSp	Ventrolateral septal nucleus	329	CB	CB	CB	0.087 ± 0.01
VM	Ventromedial thalamic nucleus	204	CB	CB	CB	0.063 ± 0.01
Vmd	Dorsal motor nucleus of the trigeminal nerve	81	CB	CB	CB	0.030 ± 0.00
Vme	Trigeminal mesencephalic tract	168	CB	CB	CB	0.002 ± 0.00
VmH	Ventromedial hypothalamic nucleus	187	CB	CB	CB	0.305 ± 0.02
VmSp	Ventromedial septal nucleus	236	CB	CB	CB	0.200 ± 0.02
Vmv	Ventral motor nucleus of the trigeminal nerve	30	CB	CB	CB	0.079 ± 0.01
Vp	Principal nucleus of the trigeminal nerve	9	CB	CB	CB	0.064 ± 0.01
VPa	Ventral pallidum	352	CB	CB	CB	0.250 ± 0.03
VPt	Ventral pretectal nucleus	148	CB	CB	CB	0.055 ± 0.01
Vs	Spinal nucleus of the trigeminal nerve	13	CB	CB	CB	0.009 ± 0.00
Vt	Tangential vestibular nucleus	54	CB	CB	CB	0.023 ± 0.00
VTA	Ventral tegmental area	130	CB	CB	CB	0.099 ± 0.01
Vvl	Ventrolateral vestibular nucleus	56	CB	CB	CB	0.027 ± 0.00
Vvm	Ventromedial vestibular nucleus	57	CB	CB	CB	0.030 ± 0.00
XII	Nucleus of the hypoglossal nerve	36	CB	CB	CB	0.116 ± 0.01
Xm	Motor nucleus of the vagus nerve	34	CB	CB	CB	0.028 ± 0.00
Xmd	Dorsal motor nucleus of the vagus nerve	32	CB	CB	CB	0.030 ± 0.01
Z	Nucleus Z	170	CB	CB	CB	0.014 ± 0.00
4v	Fourth ventricle	175	CB	CB	CB	0.702 ± 0.11
a	Alveus	326	CB	CB	CB	0.950 ± 0.12
A8	Catecholaminergic cell group A8	106	CB	CB	CB	0.127 ± 0.01

CB contrast-based, *LB* literature-based

*Transient connection from Fig. 9 to 10 in Hoops et al. (2018) is LB

+Mean volumes in µL ± 95% confidence intervals

published this century, Hoops et al. (2018) and Billings et al. (2020) are both MRI-based. Just as there is a strong desire to bring the available reference material for reptile brains up to the modern standards of other vertebrate groups, the publication of these atlases demonstrates a strong need to move reptile neuroscience—and evolutionary neuroscience more broadly—into new modalities and techniques. The 3D segmentation atlas presented here is one way we are enabling the acceleration of this progress.

Multimodal imaging

Though anatomical MRI is a powerful tool that has revealed substantial new information regarding the architecture of the vertebrate brain, increasingly large and complex neuroanatomical problems are beyond the capabilities of conventional anatomical MRI alone. Several recent neuroscience projects have used multimodal imaging techniques that combined anatomical imaging with MRI techniques that are sensitive to the microscopic organization of tissue to map the complexity of the human brain. Examples of such projects include the Human Connectome Project (Essen et al. 2013) and the BRAIN Initiative (Insel et al. 2013).

In reptile and evolutionary neuroscience, it will be necessary, moving forward, to similarly embrace multimodal imaging to further understand shifts in brain structure and function over evolution, and their causes and consequences. At its most fundamental level, this would mean the development of complementary MRI models which could be used to verify and further refine the atlas published here. Our atlas is based on a series of T2*-weighted MRI images. Other forms of MR contrast such as T1-weighted and T2-weighted images could reveal anatomical structure not evident in our T2*-weighted model.

In fact, there is a diversity of tools that we should consider combining with the atlas presented here, both within

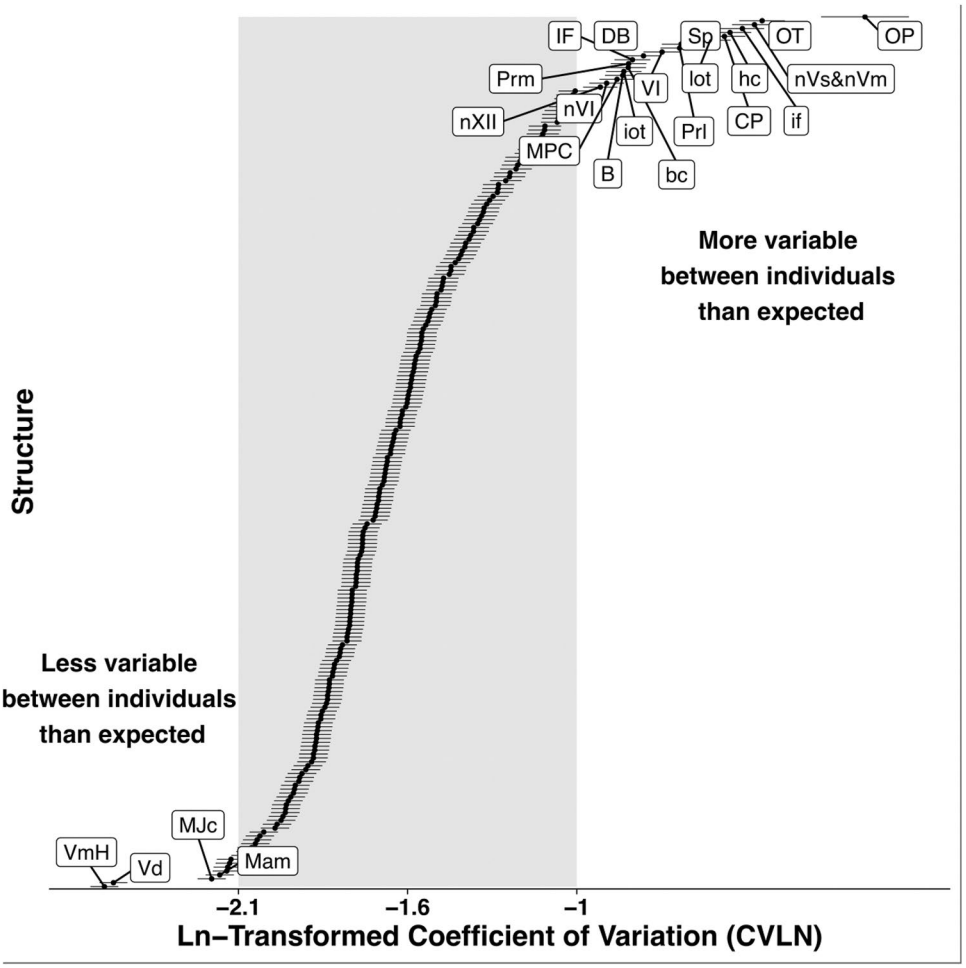

Fig. 5 This caterpillar plot (Hurley 2020) shows brain regions ranked by effect size. The 95% prediction interval is shaded in gray. Those brain regions with effect sizes below the 95% prediction interval are less variable than expected. Interestingly, two of these regions are large, adjacent regions of the tuberal hypothalamus. Brain regions with effect sizes above the 95% prediction interval are more variable than expected. The majority of these regions are rhombencephalic, which parallels the finding that the rhombencephalon is an evolutionarily labile brain region in *Ctenophorus* (Hoops et al. 2017)

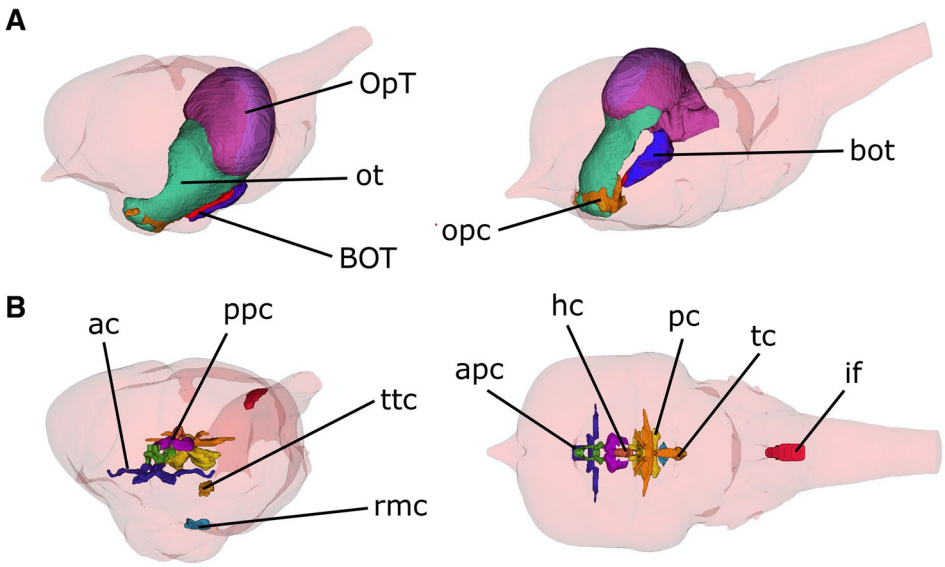

Fig. 6 Two subsets of brain structures segmented in our atlas, shown in a 3D transparent brain. **a** The optic system of the left hemisphere is shown, demonstrating how the structures are connected and fit within the brain. **b** Commissures are shown bilaterally to visualize their cross-midline connectivity. Abbreviations are defined in Table 1

three-dimensional imaging and by linking to histology. Within MRI, developing an understanding of how brain regions are connected is arguably just as important as determining where they are located. Brain mapping initiatives within mammals are working hard to understand the connectivity between brain regions, and the implications for cognition and behaviour. As an integral component of this work, it will be necessary to understand how these connections evolved and how they may evolve differently across the vertebrate phylogeny. Therefore, we place the utmost importance on developing a connectivity-based atlas (or "connectome") for the reptile brain. Such a connectome should be based on both on structural connectivity and on functional connectivity. Structural connectivity is primarily the domain of diffusion-tensor MRI, while functional connectivity is based primarily on resting-state functional MRI (Damoiseaux and Greicius 2009). Both these imaging modalities present challenges for the fine-scale resolution necessary to image the small brains of reptiles; however, advances in mouse imaging in both these modalities mean that such measurements are now becoming possible (Mechling et al. 2014; Calabrese et al. 2015). Developing these tools would dramatically increase the breadth and depth of the neuroevolutionary ideas we are able to explore.

Practically, MRI can be prohibitively expensive and time-consuming, particularly to researchers in ecology and evolution, where funding is scarce. Due to these restrictions, researchers interested in branching into neuroscience from a foundation of ecology or evolution have started working with contrast-enhanced soft-tissue computed tomography (CT; Baeckens et al. 2017). This technique allows for visualization of neuroanatomy that can exceed the resolution and approach the soft-tissue contrast of MRI, and at a much lower cost and time commitment (Crespigny et al. 2008). As CT produces 3D images, our atlas could easily be transferred onto a lizard brain model produced through CT scanning, and subsequently refined to reflect the specific contrasts visible through this imaging modality. Such a tool would broaden access to 3D neuroimaging to a larger community of researchers in the natural sciences.

Finally, it is important to develop a modern histology-based atlas of the reptile brain. Reptiles are the only vertebrate group for which new editions of modern, high-resolution histological atlases are not continuously updated and published. Generating such an atlas is critical as the vast majority of neuroanatomical methods are still histology-based. A histological atlas, particularly one that is aligned to our MRI-based atlas, would facilitate linking neuroanatomical studies to fundamental histological examinations such as tract-tracer studies, in situ hybridization, and immunohistochemistry. Linking all these modalities is the only way to develop a holistic theory of the evolution of the vertebrate brain.

Conclusion

Here, we present the first segmentation-based three-dimensional atlas of a lizard brain. This atlas is intended for general neuroanatomical localization, such as finding specific structures, for understanding the three-dimensional relationships between different structures, and for developing more diverse tools and techniques for the study of reptile and evolutionary neuroscience. We add lizards to the growing diversity of available segmentation atlases, a menagerie that is essential for using structural MRI and other three-dimensional imaging modalities to examine fundamental questions in brain evolution.

Supplementary Information The online version contains supplementary material available at https://doi.org/10.1007/s00429-021-02282-z.

Acknowledgements We are grateful for the technical assistance and expertise of Christopher Hammill, Benjamin Darwin, and Rose O'Dea. DH is grateful to his PhD supervisors, Prof. J. Scott Keogh, and Prof. Martin J. Whiting, without whom this project would not have been possible. DH thanks the Australian National Imaging Facility, Western Sydney University, and University of Queensland nodes, for imaging and processing.

Funding This work was supported by a postdoctoral fellowship to DH from the National Science and Engineering Research Council of Canada (Grant number: PDF5171462018).

Data availability All data used here are available as supplementary materials and through the Open Science Framework (OSF; https://doi.org/10.17605/OSF.IO/UJENQ).

Code availability The code used in our analyses is available as a supplementary material and through the Open Science Framework (OSF; https://doi.org/10.17605/OSF.IO/UJENQ).

Declarations

Conflict of interest All authors are conflicted, like all academics, because researcher quality, including for funding and employment opportunities, is gauged based on publication output. Other than that, all authors declare no conflicts of interest.

Ethical approval This research used only previously published data and images; no animals were used specifically for the research described herein. See Hoops et al. (2018) for ethics statement related to the data previously published and subsequently used here.

References

Baeckens S, Herrel A, Broeckhoven C, Vasilopoulou-Kampitsi M, Huyghe K, Goyens J et al (2017) Evolutionary morphology of the lizard chemosensory system. Sci Rep 7(1):1–13

Behroozi M, Billings BK, Helluy X, Manger PR, Güntürkün O, Ströckens F (2018) Functional MRI in the Nile crocodile: a new avenue for evolutionary neurobiology. Proc Biol Sci 285(1877):20180178

Billings BK, Behroozi M, Helluy X, Bhagwandin A, Manger PR, Güntürkün O et al (2020) A three-dimensional digital atlas of the Nile crocodile (*Crocodylus niloticus*) forebrain. Brain Struct Funct 225(2):683–703

Butler AB, Northcutt RG (1973) Architectonic studies of the diencephalon of *Iguana iguana* (Linnaeus). J Comp Neurol 149(4):439–462

Calabrese E, Badea A, Cofer GP, Qi Y, Johnson GA (2015) A diffusion MRI tractography connectome of the mouse brain and comparison with neuronal tracer data. Cereb Cortex 25(11):4628–4637

Chakravarty MM, Steadman P, Eede MC, Calcott RD, Gu V, Shaw P et al (2013) Performing label-fusion-based segmentation using multiple automatically generated templates. Hum Brain Mapp 34(10):2635–2654

Collins DL, Pruessner JC (2010) Towards accurate, automatic segmentation of the hippocampus and amygdala from MRI by augmenting ANIMAL with a template library and label fusion. Neuroimage 52(4):1355–1366

Corral JMD, Miralles A, Nicolau MC, Planas B, Rial RV (1990) Stereotaxic atlas for the lizard *Gallotia galloti*. Prog Neurobiol 34(3):185–196

Cruce JAF (1974) A cytoarchitectonic study of the diencephalon of the tegu lizard, *Tupinambis nigropunctatus*. J Comp Neurol 153(3):215–238

Cruce WLR, Newman DB (1981) Brain stem origins of spinal projections in the lizard *Tupinambis nigropunctatus*. J Comp Neurol 198(2):185–207

Damoiseaux JS, Greicius MD (2009) Greater than the sum of its parts: a review of studies combining structural connectivity and resting-state functional connectivity. Brain Struct Funct 213(6):525–533

de Crespigny A, Bou-Reslan H, Nishimura MC, Phillips H, Carano RAD, D'Arceuil HE (2008) 3D micro-CT imaging of the post-mortem brain. J Neurosci Methods 171(2):207–213. https://linkinghub.elsevier.com/retrieve/pii/S0165027008001611

Díaz C, Glover JC (2002) Comparative aspects of the hodological organization of the vestibular nuclear complex and related neuron populations. Brain Res Bull 57(3–4):307–312

Dickie DA, Shenkin SD, Anblagan D, Lee J, Cabez MB, Rodriguez D et al (2017) Whole brain magnetic resonance image atlases: a systematic review of existing atlases and caveats for use in population imaging. Front Neuroinform 19:11

Dorr AE, Lerch JP, Spring S, Kabani N, Henkelman RM (2008) High resolution three-dimensional brain atlas using an average magnetic resonance image of 40 adult C57Bl/6J mice. Neuroimage 42(1):60–69

Essen DCV, Smith SM, Barch DM, Behrens TEJ, Yacoub E, Ugurbil K (2013) The WU-Minn human connectome project: an overview. Neuroimage 15(80):62–79

Frey S, Pandya DN, Chakravarty MM, Bailey L, Petrides M, Collins DL (2011) An MRI based average macaque monkey stereotaxic atlas and space (MNI monkey space). Neuroimage 55(4):1435–1442

Greenberg N (1982) A forebrain atlas and stereotaxic technique for the lizard, *Anolis carolinensis*. J Morphol 174(2):217–236

Hamilton AJ, May RM, Waters EK (2015) Zoology: here be dragons. Nature 1(520):42–43

Hoops D (2015) A perfusion protocol for lizards, including a method for brain removal. MethodsX 2:165–173. https://doi.org/10.1016/j.mex.2015.03.005

Hoops D (2018) The secret caverns of the dragon's brain: current and potential contributions of lizards to evolutionary neuroscience. Brain Behav Evol 25:1–3

Hoops D, Ullmann JFP, Janke AL, Vidal-García M, Gardner TS, Dwihapsari Y et al (2017a) Sexual selection predicts brain structure in dragon lizards. J Evol Biol 30(2):244–256

Hoops D, Vidal-García M, Ullmann JFP, Janke AL, Stait-Gardner T, Duchêne DA et al (2017b) Evidence for concerted and mosaic brain evolution in dragon lizards. Brain Behav Evol 90(3):211–223

Hoops D, Desfilis E, Ullmann JFP, Janke AL, Stait-Gardner T, Devenyi GA et al (2018) A 3D MRI-based atlas of a lizard brain. J Comp Neurol 526(16):2511–2547

Hughes DF, Walker EM, Gignac PM, Martinez A, Negishi K, Lieb CS et al (2016) Rescuing perishable neuroanatomical information from a threatened biodiversity hotspot: remote field methods for brain tissue preservation validated by cytoarchitectonic analysis, immunohistochemistry, and X-ray microcomputed tomography. PLoS ONE 11(5):e0155824

Hurley JC (2020) Forrest plots or caterpillar plots? J Clin Epidemiol 121:109–110

Insel TR, Landis SC, Collins FS (2013) The NIH BRAIN initiative. Science 340(6133):687–688

Janke AL, Ullmann JFP (2015) Robust methods to create ex vivo minimum deformation atlases for brain mapping. Methods 73:18–26. http://linkinghub.elsevier.com/retrieve/pii/S1046202315000110

Luo Q, Lu H, Lu H, Senseman D, Worsley K, Yang Y et al (2009) Physiologically evoked neuronal current MRI in a bloodless turtle brain: detectable or not? Neuroimage 47(4):1268–1276

Macrì S, Savriama Y, Khan I, Di-Poï N (2019) Comparative analysis of squamate brains unveils multi-level variation in cerebellar architecture associated with locomotor specialization. Nat Commun 10(1):1–16

McLean CA, Stuart-Fox DM (2014) Geographic variation in animal colour polymorphisms and its role in speciation. Biol Rev 89(4):860–873

Mechling AE, Hübner NS, Lee H-L, Hennig J, von Elverfeldt D, Harsan L-A (2014) Fine-grained mapping of mouse brain functional connectivity with resting-state fMRI. Neuroimage 1(96):203–215

Medina LM, Marti E, Artero C, Fasolo A, Puelles L (1992) Distribution of neuropeptide Y-like immunoreactivity in the brain of the lizard *Gallotia galloti*. J Comp Neurol 319:387–405. https://onlinelibrary.wiley.com/doi/abs/10.1002/cne.903190306

Nieman BJ (2005) Anatomical phenotyping in the brain and skull of a mutant mouse by magnetic resonance imaging and computed tomography. Physiol Genom 24(2):154–162

Nomura T, Gotoh H, Ono K (2013) Changes in the regulation of cortical neurogenesis contribute to encephalization during amniote brain evolution. Nat Commun 25:4

Northcutt RG (1967) Architectonic studies of the telencephalon of *Iguana iguana*. J Comp Neurol 130(2):109–147

Powers A, Reiner A (1980) A stereotaxic atlas of the forebrain and midbrain of the eastern painted turtle (*Chrysemys picta picta*). J Hirnforsch 21(2):125–159

R Core Team (2014) R: a language and environment for statistical computing. R Foundation for Statistical Computing, London

Reiter S, Liaw H-P, Yamawaki TM, Naumann RK, Laurent G (2017) On the value of reptilian brains to map the evolution of the hippocampal formation. Brain Behav Evol 90(1):41–52

Roth TC, Krochmal AR, LaDage LD (2019) Reptilian cognition: a more complex picture via integration of neurological mechanisms,

behavioral constraints, and evolutionary context. BioEssays 41(8):1900033
Schwab ME (1979) Variation in the rhombencephalon. Biology of the reptilia: neurology B. Academic Press, pp 201–242. http://www.worldcat.org/title/biology-of-the-reptilia-neurology-b/oclc/256440081
Smeets WJAJ, Hoogland PV, Lohman AHM (1986) A forebrain atlas of the lizard *Gekko gecko*. J Comp Neurol 254(1):1–19
Stuart-Fox D, Aulsebrook A, Rankin KJ, Dong CM, McLean CA (2021) Convergence and divergence in lizard colour polymorphisms. Biol Rev 96(1):289–309
Szabo B, Noble DW, Whiting MJ (2020) Learning in non-avian reptiles 40 years on: advances and promising new directions. Biol Rev 96(2):331–356
ten Donkelaar HJ (1998) Reptiles. The central nervous system of vertebrates. Springer, pp 1315–1524. http://www.worldcat.org/title/central-nervous-system-of-vertebrates-volume-2/oclc/40948106
ten Donkelaar HJ, Bangma GC, Barbas-Henry HA, de Huizen R, Wolters JG (2012) The brain stem in a lizard, *Varanus exanthematicus*. Springer
Viechtbauer W (2010) Conducting meta-analyses in R with the metafor package. J Stat Softw 36(3):1–48
Vincent RD, Neelin P, Khalili-Mahani N, Janke AL, Fonov VS, Robbins SM et al (2016) MINC 2.0: a flexible format for multi-modal images. Front Neuroinform 10:35
Yewers MSC, Pryke S, Stuart-Fox DM (2016) Behavioural differences across contexts may indicate morph-specific strategies in the lizard *Ctenophorus decresii*. Anim Behav 111(C):329–339